

Banner appropriate to article type will appear here in typeset article

Taylor rolls on tour: Slow drift of turbulent large-scale structures in flows with continuous symmetries

Daniel Feldmann^{1†} and Marc Avila^{12‡}

¹University of Bremen, Center of Applied Space Technology and Microgravity (ZARM),
Am Fallturm 2, 28359 Bremen, Germany.

²University of Bremen, MAPEX Center for Materials and Processes,
Am Biologischen Garten 2, 28359 Bremen, Germany.

(Received xx; revised xx; accepted xx)

In Rayleigh–Bénard convection and Taylor–Couette flow cellular patterns emerge at the onset of instability and persist as large-scale coherent structures in the turbulent regime. Their long-term dynamics has been thoroughly characterised and modelled for the case of turbulent convection, whereas turbulent Taylor rolls have received much less attention. Here we present direct numerical simulations of axisymmetric Taylor–Couette flow and show a discontinuous phase-transition to spatio-temporal chaos as the system size increases. Beyond this transition, Taylor rolls suddenly undergo erratic drifts evolving on a very slow time scale. We estimate an effective diffusion coefficient for the drift and compare the dynamics to analogous motions in Rayleigh–Bénard convection and Poiseuille flow, suggesting that this spontaneous diffusive displacement of large coherent structures is common among different types of wall-bounded turbulent flows.

Key words: Taylor–Couette flow, Bénard convection, Plumes/thermals, Rotating flows

1. Introduction

The smallest eddies in turbulent flows are dictated by the fluid’s kinematic viscosity (ν) and dissipation, whereas the largest ones are shaped by the flow geometry, boundary conditions and source of driving. Very large coherent motions in the flow field (superstructures) carry a substantial part of the kinetic energy, which increases as the Reynolds number (Re) increases (Smits *et al.* 2011). Understanding their role in transport and mixing is an active field of research, with many open questions relevant for predicting and modelling environmental fluid flows (Dauxois *et al.* 2021). In systems with linear instabilities, such as Rayleigh–Bénard convection (RBC) and Taylor–Couette flow (TCF), the origin of turbulent superstructures can be traced down to the onset of hydrodynamic instability. For TCF, Taylor rolls emerge from

† Email address for correspondence: daniel.feldmann@zarm.uni-bremen.de

‡ Email address for correspondence: marc.avila@zarm.uni-bremen.de

the primary instability of circular Couette flow (Taylor 1923), and then undergo a sequence of bifurcations (Coles 1965; Fenstermacher *et al.* 1979; Prigent *et al.* 2006), which increase the spatio-temporal complexity of the flow as Re increases (Feldmann *et al.* 2023). Seemingly, they persist in the form of turbulent Taylor rolls up to the highest Re investigated to date (Lathrop *et al.* 1992; Ravelet *et al.* 2010; Huisman *et al.* 2014; Ostilla-Mónico *et al.* 2016a; Sacco *et al.* 2019). We refer to Grossmann *et al.* (2016) for a recent review of turbulent Taylor–Couette flow.

Turbulent Taylor rolls have been elucidated in experiments and direct numerical simulations (DNS) employing temporal averages of the velocity field (Dong 2007; Ravelet *et al.* 2010; Ostilla-Mónico *et al.* 2013; Huisman *et al.* 2014; Ostilla-Mónico *et al.* 2016b,a), based upon the assumptions that the rolls remain stable and do not travel in axial direction (z). In most laboratory experiments the cylinders are bounded by solid end walls, whereas in DNS axially periodic boundary conditions (BC) are usually employed. This renders z homogeneous and enables the usage of short computational domains, which typically accommodate one or two pairs of Taylor rolls (Dong 2007; Brauckmann & Eckhardt 2013; Ostilla-Mónico *et al.* 2016b,a; Sacco *et al.* 2019). In these computations, typical observation times do not exceed a few hundred convective time units. This raises the question of whether Taylor rolls remain stable and stationary up to arbitrarily long times. In cylindrical RBC cells, for example, the characteristic large-scale circulation (LSC) are known to undergo spontaneous diffusive meandering in the naturally homogeneous (i. e. azimuthal) direction (Sun *et al.* 2005; Brown & Ahlers 2006; Xi *et al.* 2006; Brown & Ahlers 2008). Slow dynamics of the LSC – clearly separated from the time scale of the turbulent fluctuations – was also shown more recently in DNS of rectangular RBC at Rayleigh numbers up to $Ra = 10^7$ (Pandey *et al.* 2018). Similarly, Kreilos *et al.* (2014) found slow spanwise displacements of velocity streaks in turbulent boundary layer and Poiseuille flows.

In this paper, we reveal a discontinuous phase-transition giving rise to slow, large-scale dynamics in axisymmetric TCF. Beyond a critical domain size, spatio-temporal chaos emerges and the Taylor rolls undergo erratic drifts in z . Compared to the cylinder rotation, the drift speeds are small, but large roll displacements can occur on a slow time scale. We show that the drift statistics are consistent with a Wiener process and characterise the motion with an effective diffusion coefficient of the order of ν .

2. Computer experiments

We perform axisymmetric DNS of Taylor–Couette flow with periodic BC in z for moderate Reynolds numbers, allowing for both, large computational domains and long integration times at affordable computing costs. We integrate the incompressible Navier–Stokes equations (subject to no-slip BC in r) forward in time (t) using our pseudo-spectral DNS code **nsCouette** (López *et al.* 2020). The equations are formulated in cylindrical coordinates (r, θ, z) and rendered dimensionless using d , ν/d and d^2/ν (i. e. the characteristic viscous time scale of the problem), as unit length, unit speed and unit time, respectively. In axisymmetric DNS, the θ -dependence is dropped, but all three velocity components are computed.

Motivated by an exact analogy (Eckhardt *et al.* 2020) between two-dimensional RBC and axisymmetric TCF in the narrow gap limit ($\eta = r_i/r_o \rightarrow 1$), we set $\eta = 0.99$ and vary $Re_s = U d/\nu$, $R\Omega = 2d\Omega/U$ and $\Gamma = L_z/d$. Here, $d = r_o - r_i$ is the gap width between the inner (i) and outer (o) cylinder, L_z is the axial length, $U = u_{\theta,i} - \eta u_{\theta,o}$ and $\Omega = u_{\theta,o}/r_o$, where $u_{\theta,i/o}$ denotes the azimuthal speed of the cylinders. An important response parameter is the Nusselt number (Nu_s), which quantifies the transport of angular momentum across the fluid layer (Eckhardt *et al.* 2007; Brauckmann *et al.* 2016; Eckhardt *et al.* 2020). In a first set of DNS, we fix all parameters, but Γ , to investigate the onset of spatio-temporal chaos with respect

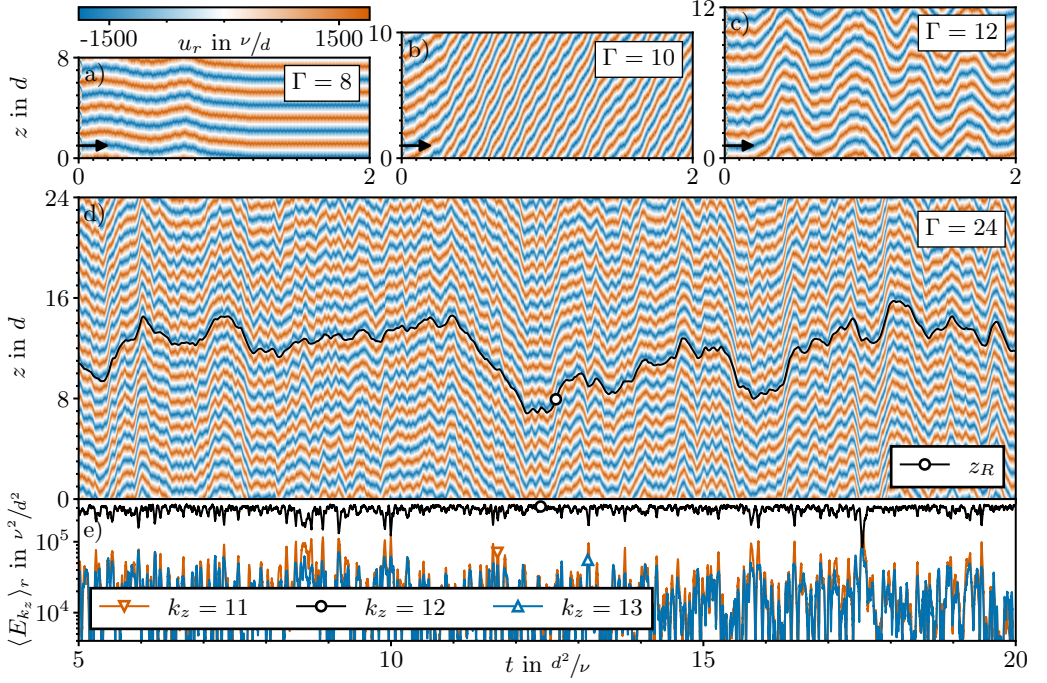


Figure 1: Spatio-temporal dynamics of Taylor rolls w. r. t. the domain size (Γ). Shown are contours of wall-normal velocities (u_r) at mid-gap extracted from DNS ($Re_s = 9475$, $R_\Omega = 0.14$). Arrows represent 2000 convective time units. a): Stationary Taylor rolls. b–d): Axial motions on a slow time scale. d): Temporal evolution of the phase angle of the dominant Fourier mode ($k_z = 12$) of u_r on top of the space-time data as a proxy for the displacement of the rolls (z_R) here for twelve pairs of rolls. e): Kinetic energy time series ($\langle E_{k_z} \rangle_r$) for mode k_z .

to the lateral domain size. In a second set (compiled in table 1), we fix Γ and explore the effect of shear (Re_s) and rotation (R_Ω). The initial conditions are chosen to trigger the desired number of Taylor rolls (N_R) necessary to maintain their aspect ratio constant throughout all DNS runs ($N_R/\Gamma = 1$). This is important because the dynamics is known to depend on N_R/Γ (Ostilla-Mónico *et al.* 2015, 2016a; Wang *et al.* 2020; Zwirner *et al.* 2020). The highest friction Reynolds number ($Re_\tau = u_\tau d/\nu$, where u_τ is the friction velocity at the cylinder walls) measured in all DNS is 408 (table 1). The spatial resolution in terms of wall units (i. e. based on Re_τ and denoted by $^+$) is at least $0.07 \leq \Delta r^+ \leq 4.03$ and $\Delta z^+ = 4.89$, which is state of the art in DNS of wall-bounded turbulence (Ostilla-Mónico *et al.* 2016b,a; Feldmann *et al.* 2021).

3. Drift dynamics

Small domains restrict the dynamics of the system, resulting in nearly stationary rolls. This is apparent from the space-time diagram of the wall-normal velocity (u_r) for $\Gamma = 8$ (figure 1a). If we now enlarge the domain ($\Gamma \geq 10$, $N_R/\Gamma = 1$), the Taylor rolls undergo large, erratic, collective drifts in z , that evolve on a slow time scale (figure 1b–d). In a domain with $N_R = 24$ rolls, for example, the most energetic axial mode is always $k_z = 12$ (figure 1e), confirming that the space-time representation of u_r is indeed a robust way to identify Taylor rolls and to track their dynamics. Every few viscous time units (e. g. at $t \approx 17.5$), the competition with neighbouring modes (here $k_z \in \{11, 13\}$) represents rare attempts to switch to another state

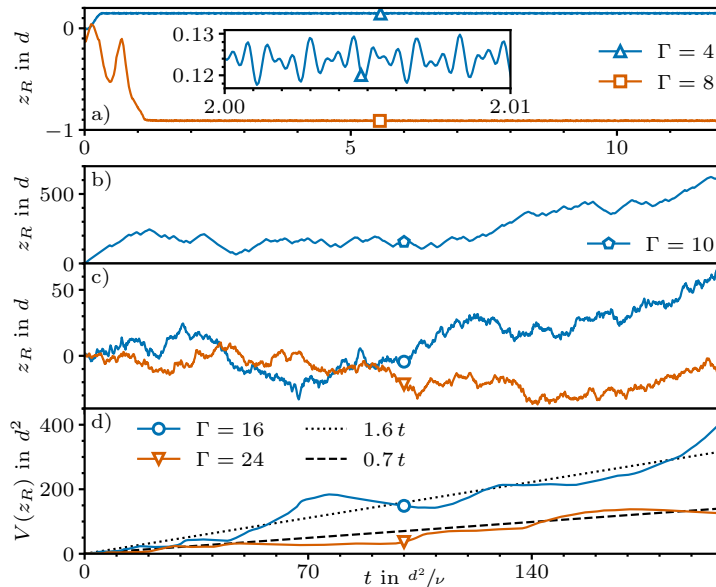


Figure 2: Time series of the axial displacement (z_R) of Taylor rolls in different domains (Γ) extracted from DNS ($Re_s = 9475$, $R_Q = 0.14$). a): Chaotic small-scale oscillations. b): Huge drifts. c): Chaotic oscillations with large erratic drifts. d): Displacement variance ($V(z_R)$) and linear fit (broken lines).

with eleven or thirteen pairs of rolls. These attempts, however, remained unsuccessful in all our simulations.

To analyse the drift dynamics quantitatively, we compute axial Fourier spectra of u_r (space-time data as in figure 1d) and use the phase angle of the axial dominant mode (here $k_z = 12$) to approximate the displacement of the rolls (z_R), as done earlier (Sacco *et al.* 2019). The temporal evolution of z_R (figure 1d) aligns well with u_r , thereby confirming the suitability of z_R to quantify the drift. For $\Gamma \leq 8$, the rolls first undergo slow transient drifts in the beginning of the simulation and then ultimately oscillate with tiny amplitudes and high frequencies about a statistically steady state (figure 2a). This fast dynamics of the rolls was reported earlier for 3d turbulent TCF in a domain accommodating one pair of rolls (Sacco *et al.* 2019). By contrast, for $\Gamma = 10$ the rolls tramp more than $100d$ before turning back for the first time, and continue moving erratically thereafter (figure 2b). With further increasing Γ , these excursions persist but become less extreme (figure 2c).

We quantify the Taylor-roll motion statistically by computing the variance of the axial displacement, $V(z_R) = \langle z_R^2 \rangle - \langle z_R \rangle^2$, where angled brackets denote temporal averaging. For $\Gamma \leq 8$ the fast dynamics of the rolls is centred around a fixed location and $V(z_R)$ quickly saturates to a constant, in agreement with Sacco *et al.* (2019), who reported Gaussian fluctuations of z_R with constant variance. By contrast, for $\Gamma \geq 10$, $V(z_R)$ grows approximately linearly with time, as in a Wiener process (figure 2d). The drift of the rolls can be thus characterised with an effective diffusion coefficient (D_R), as the slope of a linear fit to the variance. We generally discard the first $2d^2/\nu$ to exclude initial transients.

4. Discontinuous phase transition

The dependence of the diffusion coefficient on the domain size is shown in figure 3. Our data suggest a divergence of D_R near a critical point, $\Gamma_c = 9.99$, followed by a monotonous

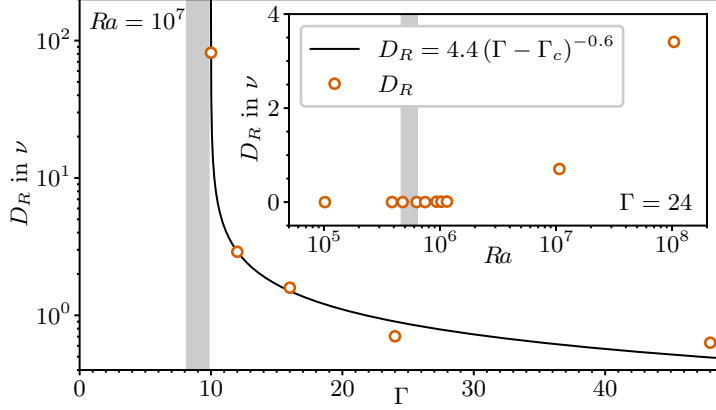


Figure 3: Phase transition for the onset of large, erratic drifts w.r.t. the domain size (Γ). Beyond the critical point (grey bar, $\Gamma_c = 9.99$ in the fit), the motion can be characterised by an effective diffusion coefficient (D_R , figure 2d). The inset compares D_R for TCF at different Rayleigh numbers (Ra).

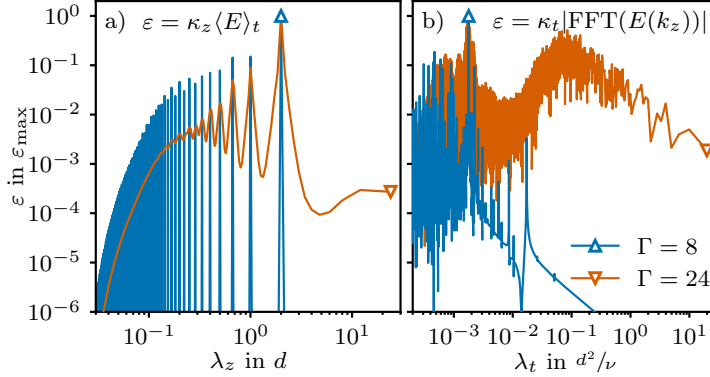


Figure 4: Transition from temporal to spatio-temporal chaos in TCF ($Re_s = 9475$, $R_Q = 0.14$) w.r.t. the domain length (Γ). a): Time averaged, premultiplied axial Fourier spectra of the u_r data (figure 1a,d) versus axial wavelengths $\lambda_z = 2\pi/\kappa_z$. b): Premultiplied temporal Fourier spectra of the modal kinetic energy (figure 1e) for the dominant mode (e.g. $k_z = 4$ for $\Gamma = 8$) versus temporal wavelengths $\lambda_t = 2\pi/\kappa_t$.

decrease as Γ increases. To examine the nature of this discontinuous transition, we compare spatial and temporal Fourier spectra from sub- and super-critical domains (figure 4). For $\Gamma = 8$, the axial spectrum of u_r presents discrete peaks at wavelength $\lambda_z = 2d$ and its harmonics only (figure 4a). This implies that the flow state consists of four perfectly synchronised copies of one pair of Taylor rolls. In fact, when comparing this state to those obtained for $\Gamma \in \{2, 4\}$, the same Nusselt numbers ($\langle Nu_s \rangle = 12.82476$) and spectra (not shown) are recovered. By contrast, the states obtained for $\Gamma \geq 10$ exhibit continuous spatial spectra (e.g. $\Gamma = 24$ in figure 4a), indicating spatial defects in the roll structure; i.e. there are no identical rolls in the entire stack. A similar transition to spatio-temporal chaos was reported before for axially oscillated (Avila *et al.* 2007) and hydromagnetic (Guseva *et al.* 2015) TCF. For both, however, no slow large-scale drift of the roll patterns was reported, possibly due to much shorter simulation times.

The transition to spatio-temporal chaos also alters the temporal spectra (figure 4b). For $\Gamma < \Gamma_c$, the temporal spectrum is continuous, indicating temporal chaos, and exhibits a peak

Ra	Re_s	R_Ω	Nu_s	Nu	Re_τ	$V(v_R)^{1/2}$	$V(\bar{u}_z)^{1/2}$	D_R
10^5	925	0.14	4.5		32	10^{-14}	10^{-13}	10^{-29}
10^6	2940	0.14	7.4		74	0.4	1.1	0.008
10^7	7138	0.30	10.4	14.4	137	6.4	8.8	0.4
10^7	9475	0.14	12.8	14.7	175	6.3	8.8	0.7
10^7	9475	0.14	12.8		175	2.2	NOFX	0.07
10^7	15 779	0.05	14.6	15.3	241	8.0	10.5	2
10^8	29 539	0.14	22.4		408	12.0	13.8	3

Table 1: Taylor roll dynamics in different set-ups ($\Gamma = 24$). Listed are control parameters (Ra , Re_s , R_Ω), response parameters (Nu_s , Nu , Re_τ), standard deviations of the drift speed (v_R), net axial flux (\bar{u}_z), and the effective diffusion coefficient (D_R). NOFX means $\bar{u}_z = 0$ enforced.

at about 20 convective time units before sharply falling. This peak is associated to the fast, small-displacement dynamics with $D_R = 0$ reported by Sacco *et al.* (2019). For $\Gamma > \Gamma_c$, the temporal spectrum features an additional broad peak at about $0.1d^2/\nu$, corresponding to the slow drift dynamics characterised by a Wiener process. The transition to spatio-temporal chaos is also reflected in the mean Nusselt number, but only in the third digit ($\langle Nu_s \rangle = 12.78 \pm 0.04$ for all Γ). We note that while much effort has been dedicated to remove drifts in the analysis of turbulent dynamics of wall-bounded flows (Willis *et al.* 2013; Budanur *et al.* 2015), here the onset of spatio-temporal chaos appears intrinsically linked to the slow, erratic drift dynamics.

5. Dependence of the drift dynamics on the flow configuration

We exploit the analogy between TCF and RBC (Bradshaw 1969; Veronis 1970; Prigent *et al.* 2006; Eckhardt *et al.* 2007, 2020), to demonstrate that the drift dynamics is found throughout the centrifugally unstable co-rotating regime. According to the exact Navier–Stokes mapping of Eckhardt *et al.* (2020), axisymmetric TCF systems in the narrow-gap limit ($\eta \rightarrow 1$) are exactly identical if $Ra = Re_s^2 R_\Omega (1 - R_\Omega) = \text{const.}$; i.e. the large-scale drift dynamics is identical as well. Indeed, for moderate outer cylinder rotation ($R_\Omega \in \{0.14, 0.30\}$), the drift statistics are similar (table 1) and the same is true for the corrected Nusselt number ($Nu = 1 + Nu_s - 1/1 - R_\Omega$) (Eckhardt *et al.* 2020). We attribute the small deviations to small, yet finite, curvature effects ($\eta = 0.99 < 1$), which are not included in the analogy. For very slow outer cylinder rotation ($R_\Omega = 0.05$), the drift statistics deviate noticeably. This is as expected, because the exact analogy breaks down in the limit of a stationary outer cylinder ($R_\Omega = 0$). Next, we fix R_Ω and vary Re_s . As Re_s increases, the rolls become more active. Specifically, the variance of the drift speed, $V(v_R) = V(\dot{z}_R) = \langle \dot{z}_R^2 \rangle - \langle \dot{z}_R \rangle^2$, increases as Re_s increases (table 1 and inset in figure 3). This is consistent with RBC experiments (Xi *et al.* 2006), where the rate of erratic rotation of the LSC increases tenfold as Ra increases from 10^9 to 10^{10} .

The axial drift of the Taylor rolls is associated to a net mass flux in z with mean speed \bar{u}_z . This flux is strongly correlated to the drift speed (v_R) of the rolls (figure 5a), and raises the question of whether the roll displacement causes the net axial flux or vice versa. The fact that v_R is approximately $500d/\nu$ ahead of \bar{u}_z suggests the former (figure 5b). We probe this hypothesis by enforcing $\bar{u}_z = 0$, as in laboratory experiments of TCF with end-walls. In our DNS with axially periodic BC, we enforce $\bar{u}_z = 0$ by imposing an appropriate adverse

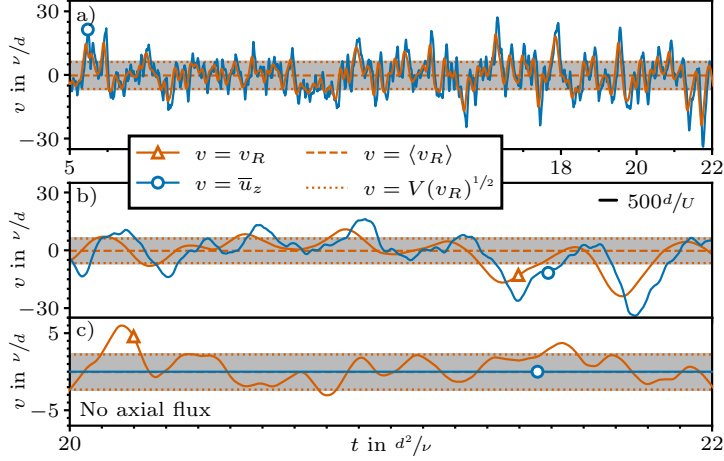


Figure 5: Taylor roll dynamics in DNS ($Re_s = 9475$, $R_\Omega = 0.14$, $\Gamma = 24$) with and w/o axial flux constraint. a): Time series of the drift speed (v_R) and the net axial flux (\bar{u}_z) for the case in figure 1d. b): Zoom of a). Dash represents 500 convective time units. c): Time series from DNS with $\bar{u}_z = 0$ enforced.

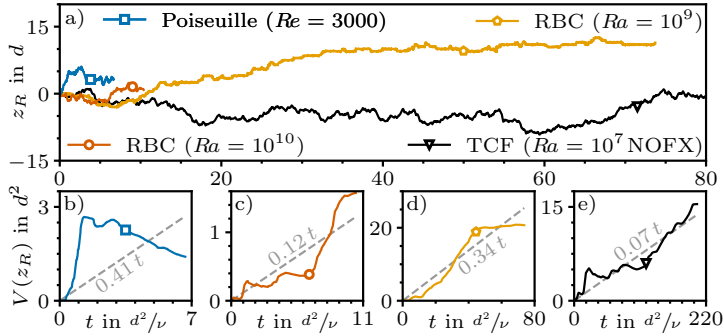


Figure 6: Large-scale drift (z_R) in different systems. a): Axial Taylor roll drift in TCF w/o net axial flux (NOFX). Azimuthal meandering of single convection rolls in cylindrical RBC cells; eleven ($Ra = 10^{10}$ (Brown & Ahlers 2006)) and 33 ($Ra = 10^9$ (Xi *et al.* 2006)) days lab experiments. Spanwise streak displacement in Poiseuille flow DNS (Kreilos *et al.* 2014). b–e): Corresponding displacement variance ($V(z_R)$) including linear fits (broken lines) to estimate an effective diffusion coefficient.

pressure gradient at each time-step. This technique was previously applied to successfully compare axially periodic simulations to lab experiments for Taylor–Couette flow with radial heating (Ali & Weidman 1990) and axially oscillating inner cylinder (Marques & Lopez 1997). As a result of suppressing the axial mass flux, v_R , $V(v_R)$ and D_R are substantially reduced (figure 5c, table 1), but when rescaled, the drift dynamics remains qualitatively unaltered (figure 6a). Specifically, $V(z_R)$ still increases linearly with time (figure 6e), although at a slower pace.

6. Discussion

We have shown that axisymmetric Taylor–Couette flows exhibit a phase transition to spatio-temporally chaotic Taylor rolls that drift erratically in the axial direction. At long time scales, the drift motion is diffusive and can lead to very large displacements. Future works

should clarify whether this dynamics persists in three-dimensional TCF simulations and in experiments with end-walls. We note that even with walls, flow patterns can drift in z with phase being created/annihilated near the walls (Heise *et al.* 2008).

The roll displacements extracted from our DNS are compared to the meandering of the LSC in RBC (Brown & Ahlers 2006; Xi *et al.* 2006) and to spanwise streak displacements in Poiseuille flow (Kreilos *et al.* 2014) in figure 6. For the sake of comparison, we converted the rotation angle to a length as $z_R(t) = R\theta(t)$ using the radius (R) of the RBC cell. Additionally, we rescaled all drift signals to the viscous time unit, which is also the relevant one of the exact analogy (Eckhardt *et al.* 2020). The qualitative agreement is remarkable and suggests that this slow dynamics might be inherent to large-scale motions in many fluid systems. However, longer RBC and Poiseuille flow runs would be needed to confirm the Wiener statistics found here for TCF, and to estimate the corresponding diffusion coefficients (figure 6b–e). Additional statistical analyses and modelling strategies previously applied to three-dimensional RBC (Brown & Ahlers 2007, 2008) could help elucidate further aspects of the drift dynamics reported here and deepen this comparison.

We stress that the shortest time series considered here (figure 2) correspond to $200Re_s = O(10^6)$ convective time units and to $200\sqrt{Ra} = O(10^5)$ free-fall time units in RBC ($Ra = 10^7$). These observation times are comparable to those used to characterise large-scale states in RBC (Pandey *et al.* 2018; Wang *et al.* 2020), but they are several orders of magnitudes longer compared to typical observation times in high- Re TCF studies (Brauckmann & Eckhardt 2013; Huisman *et al.* 2014; Ostilla-Mónico *et al.* 2016b,a; Sacco *et al.* 2019). In the Taylor–Couette apparatus of Huisman *et al.* (2014), for example, this would correspond to a measurement time of two weeks.

Acknowledgements. We appreciate stimulating discussions with Alberto Vela-Martín and Daniel Morón and we gratefully acknowledge the received funding.

Funding. We received financial support from the German Research Foundation (DFG) through the priority programme [Turbulent Superstructures \(SPP1881\)](#) and computational resources provided by the [North German Supercomputing Alliance \(HLRN\)](#) through project hbi00041.

Declaration of interests. The authors report no conflict of interest.

Data availability statement. The data that support the findings of this study will be made openly available in [Pangaea](#) at <http://doi.org> . . .

Author ORCIDs. Daniel Feldmann, <https://orcid.org/0000-0002-6585-2875>; Marc Avila, <https://orcid.org/0000-0001-5988-1090>

REFERENCES

- ALI, MOHAMED & WEIDMAN, P. D. 1990 On the stability of circular Couette flow with radial heating. *Journal of Fluid Mechanics* **220**, 53–84.
- AVILA, MARC, MARQUES, FRANCISCO, LOPEZ, JUAN M. & MESEGUER, ALVARO 2007 Stability control and catastrophic transition in a forced Taylor–Couette system. *Journal of Fluid Mechanics* **590**, 471–496.
- BRADSHAW, P. 1969 The analogy between streamline curvature and buoyancy in turbulent shear flow. *Journal of Fluid Mechanics* **36** (1), 177–191.
- BRAUCKMANN, HANNES J. & ECKHARDT, BRUNO 2013 Direct numerical simulations of local and global torque in Taylor–Couette flow up to $Re = 30\,000$. *Journal of Fluid Mechanics* **718**, 398–427.
- BRAUCKMANN, HANNES J., SALEWSKI, MATTHEW & ECKHARDT, BRUNO 2016 Momentum transport in Taylor–Couette flow with vanishing curvature. *Journal of Fluid Mechanics* **790**, 419–452.
- BROWN, ERIC & AHLERS, GUENTER 2006 Rotations and cessations of the large-scale circulation in turbulent Rayleigh–Bénard convection. *Journal of Fluid Mechanics* **568**, 351.
- BROWN, ERIC & AHLERS, GUENTER 2007 Large-Scale Circulation Model for Turbulent Rayleigh–Bénard Convection. *Physical Review Letters* **98** (13), 134501.

- BROWN, ERIC & AHLERS, GUENTER 2008 A model of diffusion in a potential well for the dynamics of the large-scale circulation in turbulent Rayleigh–Bénard convection. *Physics of Fluids* **20** (7), 075101.
- BUDANUR, NAZMI BURAK, CVITANOVIĆ, PREDRAG, DAVIDCHACK, RUSLAN L. & SIMINOS, EVANGELOS 2015 Reduction of $SO(2)$ symmetry for spatially extended dynamical systems. *Physical Review Letters* **114** (8), 1–5.
- COLES, DONALD 1965 Transition in circular Couette flow. *Journal of Fluid Mechanics* **21** (3), 385–425.
- DAUXOIS, T., PEACOCK, T., BAUER, P., CAULFIELD, C. P., CENEDESE, C., GORLÉ, C., HALLER, G., IVEY, G. N., LINDEN, P. F., MEIBURG, E., PINARDI, N., VRIEND, N. M. & WOODS, A. W. 2021 Confronting Grand Challenges in environmental fluid mechanics. *Physical Review Fluids* **6** (2), 020501.
- DONG, S. 2007 Direct numerical simulation of turbulent Taylor–Couette flow. *Journal of Fluid Mechanics* **587**, 373–393.
- ECKHARDT, BRUNO, DOERING, CHARLES R. & WHITEHEAD, JARED P. 2020 Exact relations between Rayleigh–Bénard and rotating plane Couette flow in two dimensions. *Journal of Fluid Mechanics* **903** (Busse 2012), R4.
- ECKHARDT, BRUNO, GROSSMANN, SIEGFRIED & LOHSE, DETLEF 2007 Fluxes and energy dissipation in thermal convection and shear flows. *Europhysics Letters (EPL)* **78** (2), 24001.
- FELDMANN, DANIEL, BORRERO-ECHEVERRY, DANIEL, BURIN, MICHAEL J., AVILA, KERSTIN & AVILA, MARC 2023 Routes to turbulence in Taylor–Couette flow. *Philosophical Transactions of the Royal Society A: Mathematical, Physical and Engineering Sciences* **381** (2246).
- FELDMANN, DANIEL, MORÓN, DANIEL & AVILA, MARC 2021 Spatiotemporal intermittency in pulsatile pipe flow. *Entropy* **23** (1), 1–19.
- FENSTERMACHER, P. R., SWINNEY, HARRY L. & GOLLUB, J. P. 1979 Dynamical instabilities and the transition to chaotic Taylor vortex flow. *Journal of Fluid Mechanics* **94** (1), 103–128.
- GROSSMANN, SIEGFRIED, LOHSE, DETLEF & SUN, CHAO 2016 High-Reynolds Number Taylor-Couette Turbulence. *Annual Review of Fluid Mechanics* **48**, 53–80.
- GUSEVA, ANNA, WILLIS, ASHLEY P., HOLLERBACH, RAINER & AVILA, MARC 2015 Transition to magnetorotational turbulence in Taylor-Couette flow with imposed azimuthal magnetic field. *New Journal of Physics* **17** (9).
- HEISE, M., HOFFMANN, CH, ABSHAGEN, J., PINTER, A., PFISTER, G. & LÜCKE, M. 2008 Stabilization of Domain Walls between Traveling Waves by Nonlinear Mode Coupling in Taylor-Couette Flow. *Physical Review Letters* **100** (6), 064501.
- HUISMAN, SANDER G., VAN DER VEEN, ROELAND C.A., SUN, CHAO & LOHSE, DETLEF 2014 Multiple states in highly turbulent Taylor-Couette flow. *Nature Communications* **5** (May), 1–5.
- KREILOS, TOBIAS, ZAMMERT, STEFAN & ECKHARDT, BRUNO 2014 Comoving frames and symmetry-related motions in parallel shear flows. *Journal of Fluid Mechanics* **751**, 685–697.
- LATHROP, DANIEL P, FINEBERG, JAY & SWINNEY, HARRY L 1992 Transition to shear-driven turbulence in Couette-Taylor flow. *Physical Review A* **46** (10), 6390–6405.
- LÓPEZ, JOSE MANUEL, FELDMANN, DANIEL, RAMPP, MARKUS, VELA-MARTÍN, ALBERTO, SHI, LIANG & AVILA, MARC 2020 nsCouette – A high-performance code for direct numerical simulations of turbulent Taylor–Couette flow. *SoftwareX* **11**, 100395.
- MARQUES, FRANCISCO & LOPEZ, JUAN M. 1997 Taylor–Couette flow with axial oscillations of the inner cylinder: Floquet analysis of the basic flow. *Journal of Fluid Mechanics* **348**, 153–175.
- OSTILLA-MÓNICO, RODOLFO, LOHSE, DETLEF & VERZICCO, ROBERTO 2016a Effect of roll number on the statistics of turbulent Taylor-Couette flow. *Physical Review Fluids* **1** (5), 054402.
- OSTILLA-MÓNICO, RODOLFO, STEVENS, RICHARD J.A.M., GROSSMANN, SIEGFRIED, VERZICCO, ROBERTO & LOHSE, DETLEF 2013 Optimal Taylor-Couette flow: Direct numerical simulations. *Journal of Fluid Mechanics* **719**, 14–46.
- OSTILLA-MÓNICO, RODOLFO, VERZICCO, ROBERTO, GROSSMANN, SIEGFRIED & LOHSE, DETLEF 2016b The near-wall region of highly turbulent Taylor-Couette flow. *Journal of Fluid Mechanics* **788**, 95–117.
- OSTILLA-MÓNICO, RODOLFO, VERZICCO, ROBERTO & LOHSE, DETLEF 2015 Effects of the computational domain size on direct numerical simulations of Taylor-Couette turbulence with stationary outer cylinder. *Physics of Fluids* **27** (2), 025110.
- PANDEY, AMBRISH, SCHEEL, JANET D. & SCHUMACHER, JÖRG 2018 Turbulent superstructures in Rayleigh–Bénard convection. *Nature Communications* **9** (1), 1–11.
- PRIGENT, ARNAUD, DUBRULLE, BÉRENGÈRE, DAUCHOT, OLIVIER & MUTABAZI, INNOCENT 2006 The Taylor-Couette Flow: The Hydrodynamic Twin of Rayleigh–Bénard Convection. In *Dynamics of Spatio-*

- Temporal Cellular Structures* (ed. Innocent Mutabazi, José Eduardo Wesfreid & Etienne Guyon), *Springer Tracts in Modern Physics*, vol. 207, pp. 225–242. Springer New York.
- RAVELET, F., DELFOS, R. & WESTERWEEL, J. 2010 Influence of global rotation and Reynolds number on the large-scale features of a turbulent Taylor-Couette flow. *Physics of Fluids* **22** (5), 1–8.
- SACCO, FRANCESCO, VERZICCO, ROBERTO & OSTILLA-MÓNICO, RODOLFO 2019 Dynamics and evolution of turbulent Taylor rolls. *Journal of Fluid Mechanics* **870**, 970–987.
- SMITS, ALEXANDER J., MCKEON, BEVERLEY J. & MARUSIC, IVAN 2011 High-Reynolds number wall turbulence. *Annual Review of Fluid Mechanics* **43**, 353–375.
- SUN, CHAO, XI, HENG-DONG & XIA, KE-QING 2005 Azimuthal Symmetry, Flow Dynamics, and Heat Transport in Turbulent Thermal Convection in a Cylinder with an Aspect Ratio of 0.5. *Physical Review Letters* **95** (7), 074502.
- TAYLOR, GEOFFREY INGRAM 1923 Stability of a viscous liquid contained between two rotating cylinders. *Philosophical Transactions of the Royal Society of London. Series A, Containing Papers of a Mathematical or Physical Character* **223** (605-615), 289–343.
- VERONIS, GEORGE 1970 The Analogy Between Rotating and Stratified Fluids. *Annual Review of Fluid Mechanics* **2** (1), 37–66.
- WANG, QI, VERZICCO, ROBERTO, LOHSE, DETLEF & SHISHKINA, OLGA 2020 Multiple States in Turbulent Large-Aspect-Ratio Thermal Convection: What Determines the Number of Convection Rolls? *Physical Review Letters* **125** (7), 074501.
- WILLIS, ASHLEY P., CVITANOVIĆ, PREDRAG & AVILA, MARC 2013 Revealing the state space of turbulent pipe flow by symmetry reduction. *Journal of Fluid Mechanics* **721**, 514–540.
- XI, HENG-DONG, ZHOU, QUAN & XIA, KE-QING 2006 Azimuthal motion of the mean wind in turbulent thermal convection. *Physical Review E* **73** (5), 056312.
- ZWIRNER, LUKAS, TILGNER, ANDREAS & SHISHKINA, OLGA 2020 Elliptical Instability and Multiple-Roll Flow Modes of the Large-Scale Circulation in Confined Turbulent Rayleigh-Bénard Convection. *Physical Review Letters* **125** (5), 054502.